IVYSPRING INTERNATIONAL PUBLISHER

Theranostics

2016; 6(6): 849-861. doi: 10.7150/thno.14744

Research Paper

Towards Personalized Treatment of Prostate Cancer: PSMA I&T, a Promising Prostate-Specific Membrane Antigen-Targeted Theranostic Agent

Kristell L.S. Chatalic[1,2,3]*, Sandra Heskamp[4]*, Mark Konijnenberg[1], Janneke D.M. Molkenboer-Kuenen[4], Gerben M. Franssen[4], Marian C. Clahsen-van Groningen[5], Margret Schottelius[6], Hans-Jürgen Wester[6], Wytske M. van Weerden[3], Otto C. Boerman[4], Marion de Jong[1,2]✉

1. Department of Nuclear Medicine, Erasmus MC Rotterdam, The Netherlands;
2. Department of Radiology, Erasmus MC Rotterdam, The Netherlands;
3. Department of Urology, Erasmus MC, Rotterdam, The Netherlands;
4. Department of Radiology and Nuclear Medicine, Radboud University Medical Center, Nijmegen, The Netherlands;
5. Department of Pathology, Erasmus MC, Rotterdam, The Netherlands.
6. Pharmaceutical Radiochemistry, Technische Universität München, Garching, Germany.

*These authors contributed equally to this work.

✉ Corresponding author: Marion de Jong, Erasmus MC, Department of Nuclear Medicine/Radiology, Na-610, Postbus 2040, 3000 CA Rotterdam, The Netherlands. E-mail: m.hendriks-dejong@erasmusmc.nl.

© Ivyspring International Publisher. Reproduction is permitted for personal, noncommercial use, provided that the article is in whole, unmodified, and properly cited. See http://ivyspring.com/terms for terms and conditions.

Received: 2015.12.18; Accepted: 2016.02.26; Published: 2016.04.12

Abstract

Prostate-specific membrane antigen (PSMA) is a well-established target for nuclear imaging and therapy of prostate cancer (PCa). Radiolabeled small-molecule PSMA inhibitors are excellent candidates for PCa theranostics—they rapidly and efficiently localize in tumor lesions. However, high tracer uptake in kidneys and salivary glands are major concerns for therapeutic applications. Here, we present the preclinical application of PSMA I&T, a DOTAGA-chelated urea-based PSMA inhibitor, for SPECT/CT imaging and radionuclide therapy of PCa. ^{111}In-PSMA I&T showed dose-dependent uptake in PSMA-expressing tumors, kidneys, spleen, adrenals, lungs and salivary glands. Coadministration of 2-(phosphonomethyl)pentane-1,5-dioic acid (2-PMPA) efficiently reduced PSMA-mediated renal uptake of ^{111}In-PSMA I&T, with the highest tumor/kidney radioactivity ratios being obtained using a dose of 50 nmol 2-PMPA. SPECT/CT clearly visualized subcutaneous tumors and sub-millimeter intraperitoneal metastases; however, high renal and spleen uptake in control mice (no 2-PMPA) interfered with visualization of metastases in the vicinity of those organs. Coadministration of 2-PMPA increased the tumor-to-kidney absorbed dose ratio during ^{177}Lu-PSMA I&T radionuclide therapy. Hence, at equivalent absorbed dose to the tumor (36 Gy), coinjection of 2-PMPA decreased absorbed dose to the kidneys from 30 Gy to 12 Gy. Mice injected with ^{177}Lu-PSMA I&T only, showed signs of nephrotoxicity at 3 months after therapy, whereas mice injected with ^{177}Lu-PSMA I&T + 2-PMPA did not. These data indicate that PSMA I&T is a promising theranostic tool for PCa. PSMA-specific uptake in kidneys can be successfully tackled using blocking agents such as 2-PMPA.

Key words: PSMA; imaging; SPECT; radionuclide therapy; prostate cancer; CRPC; 2-PMPA.

Introduction

Prostate cancer (PCa) is a major health problem in men. Prognosis is dependent on stage of the disease and the five-year survival rate for advanced, disseminated PCa is only 29% [1]. Metastatic castration-resistant PCa (mCRPC) is associated with poor prognosis and diminished quality of life.

Curium US LLC, Exhibit 1042
IPR2025-01582

Treatment options for mCRPC patients include taxane-based therapies (docetaxel, cabazitaxel) and novel second-line hormonal therapies (enzalutamide and abiterone), all showing moderate survival benefits. Unfortunately, those therapies are only temporarily effective and development of treatment resistance is observed [2, 3]. The bone-seeking alpha-emitting radiopharmaceutical Radium-223 chloride (Xofigo™) has recently been introduced, resulting in reduction of bone pain and moderately improved survival in mCRPC patients with bone metastases [4, 5]. However, the use of this promising radiopharmaceutical is limited to the treatment of bone metastases. Therefore, there is an urgent need to develop more specific therapies that target PCa visceral lesions as well.

Recent developments in PCa-targeted radiopharmaceuticals have focused on prostate-specific membrane antigen (PSMA) ligands. PSMA is a favorable target for imaging and radionuclide therapy of PCa, because it is overexpressed in 90-100% of local PCa lesions, as well as in cancerous lymph node metastases and bone lesions. Furthermore, reports indicate that PSMA expression levels are further enhanced in high-grade, metastatic and castration-resistant PCa [6-9].

Numerous studies have shown the value of radiolabeled PSMA-targeted agents to visualize PCa lesions, including PCa metastases [10-18]. Among the different PSMA-targeting tracers available, several tracers have made their way to the clinic. For PET imaging of PCa, Glu-NH-CO-NH-Lys-(Ahx)-^{68}Ga-HBED-CC, also known as ^{68}Ga-PSMA-11 or ^{68}Ga-PSMA-HBED-CC, is the most commonly used compound [14, 18]. Unfortunately, HBED-CC (N,N′-bis[2-hydroxy-5-(carboxyethyl)benzyl] ethylenediamine-N,N′-diacetic acid), the chelator used in this tracer, is not suitable for radiolabeling with radiometals for therapeutic applications (e.g. ^{177}Lu, ^{90}Y, ^{213}Bi). More recently, a novel ^{18}F-labeled PSMA inhibitor, ^{18}F-DCFPyL, was introduced in the clinic [19]. For therapy, anti-PSMA monoclonal antibodies (J591) radiolabeled with ^{177}Lu and ^{90}Y [11, 20, 21] and the small-molecule PSMA inhibitor [^{131}I]MIP-1095 [22] have shown promising therapeutic efficacy, although with moderate toxicity. Moreover, PSMA ligands with DOTA-derived chelators have been developed, which can be labeled with diagnostic radionuclides, e.g. ^{68}Ga for PET and ^{111}In for SPECT, as well as therapeutic radionuclides, e.g. ^{177}Lu, ^{90}Y or ^{213}Bi for radionuclide therapy. Such theranostic compounds, i.e. PSMA I&T and PSMA-617 (Fig. 1), are of great interest because they combine the potential of diagnosis and radionuclide therapy using one PSMA targeting molecule [23-27].

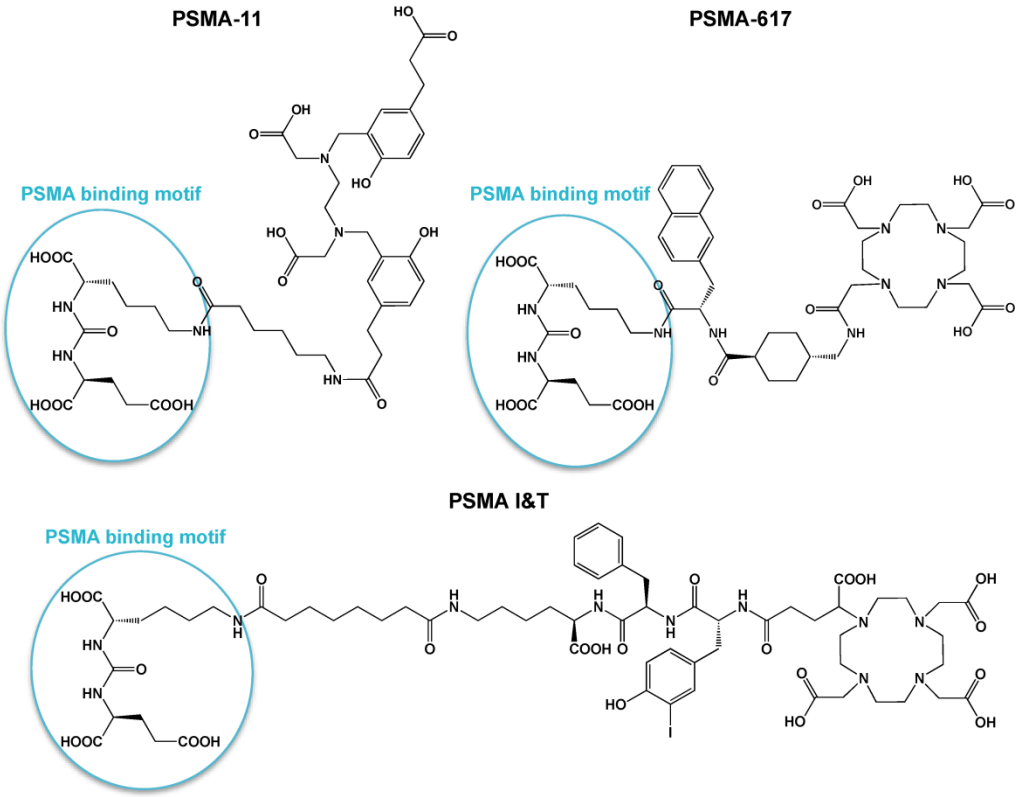

Figure 1. Chemical structures of small-molecule PSMA inhibitors PSMA-11, PSMA-617, and PSMA I&T.

Radioligand properties, e.g. lipophilicity, target affinity and metabolic stability have been carefully optimized for theranostic applications. Monoclonal antibodies showed slow blood clearance, which may result in myelotoxicity. Small-molecule PSMA inhibitors showed the advantage to localize rapidly in tumor lesions, including soft-tissue and bone metastases. On the other hand, these small inhibitors showed high and specific uptake in PSMA-expressing kidneys and salivary glands, which is of major concern for its application for radionuclide therapy. Strategies should therefore be investigated to limit radiation-induced damage in healthy organs. Here we report on the preclinical application of the DOTAGA-chelated urea-based PSMA inhibitor PSMA I&T for SPECT/CT imaging and radionuclide therapy of PCa. In this study we investigated if coinjection of ^{111}In-PSMA I&T with 2-(phosphonomethyl)pentane-1,5-dioic acid (2-PMPA) could contribute to increasing tumor-to-kidney uptake ratio, thereby facilitating visualization of metastatic lesions in the vicinity of the kidneys, and most importantly reducing toxicity during radionuclide therapy.

Materials and Methods

Cell culture

Cell lines were purchased from the American Type Culture Collection. The human prostate cancer cell line LNCaP was cultured in RPMI 1640 medium (GIBCO, BRL Life Sciences Technologies, The Netherlands), supplemented with 2 mM glutamine (GIBCO) and 10% fetal calf serum (FCS, Sigma-Aldrich Chemie BV, The Netherlands) at 37 °C in a humidified atmosphere with 5% CO_2. LS174T colon carcinoma cells were stably transfected with human PSMA using the plasmid pcDNA3.1-hPSMA and cultured in RPMI 1640 medium supplemented with 2 mM glutamine, 10% FCS, and 0.3 mg/ml G418 [28]. VCaP cells were cultured in RPMI 1640 medium containing 10% FCS. PC-346C cells were cultured in Dulbecco's modified Eagle's F12 medium supplemented with 2% FCS, 0.01% BSA (Boehringer-Mannheim), 1% insulin-transferrin-selenium (Life Technologies), 0.1 µg/mL fibronectin (Alfa Aesar), 0.1 nM R1881 androgen, 10 ng/mL epidermal growth factor, 0.5 µg/mL dexametason, 1 nM triiodothyronine, 0.1 mM phosphoethanolamine, 50 ng/mL cholera toxin and 20 µg/mL fetuin (all from Sigma).

Radiolabeling

^{111}In labeling

PSMA I&T (Fig. 1), a DOTAGA-chelated urea-based PSMA inhibitor, was synthetized as described previously [25] and kindly provided by the Technical University Munich. PSMA I&T was radiolabeled with $^{111}InCl_3$ (Mallinckrodt BV, Petten, The Netherlands) in 0.5 M 2-(N-morpholino) ethanesulfonic acid (MES) buffer (twice volume of $^{111}InCl_3$), pH 5.5, for 10 min at 95 °C under metal-free conditions [29]. After incubation, 4 mM diethylenetriaminepentaacetic acid (DTPA) was added to a final concentration of 0.2 mM to complex free $^{111}InCl_3$. Labeling efficiency was determined by instant thin-layer chromatography (ITLC) using silica gel coated paper (Agilent Technologies, Palo Alto, CA) and 0.1 M ammonium acetate containing 0.1 M ethylenediaminetetraacetic acid (EDTA), pH 5.5, as the mobile phase. Labeling efficiency exceeded 95% in all experiments.

^{177}Lu labeling

No-carrier added (n.c.a.) $^{177}LuCl_3$ was obtained from Isotope Technologies Garching (ITG) GmbH (Garching, Germany). Labeling was performed in 0.5 M MES buffer (twice volume of $^{177}LuCl_3$), pH 5.5, for 20 min at 95 °C. EDTA was added to a final concentration of 5 mM to complex free $^{177}Lu^{3+}$ after reaction. Labeling efficiency was determined by ITLC and radiochemical purity by reverse-phase high performance liquid chromatography (RP-HPLC) on an Agilent 1200 system (Agilent Technologies). A monolithic C18 column (Onyx, 4.6 x 100 mm; Phenomenex, Torrance, CA) was used at a flow rate of 1 ml/min with the following buffer system: buffer A, 0.1% v/v TFA in water; buffer B, 0.1% v/v TFA in acetonitrile; and a gradient of 97% to 0% buffer A (5-15 min). The radioactivity of the eluate was monitored using an in-line NaI radiodetector (Raytest GmbH, Straubenhardt, Germany). Elution profiles were analyzed using Gina-star software (version 2.18; Raytest GmbH). Labeling efficiency was 95% and radiochemical purity was 93-95%.

Scatchard analysis of PSMA I&T

Scatchard analysis was performed to determine the dissociation constant (K_d) of ^{111}In-PSMA I&T and to quantitatively measure PSMA expression on LNCaP and LS174T-PSMA cells. Cells were cultured to confluence in six-well plates and incubated for 4 h on ice with increasing concentrations ^{111}In-PSMA I&T (0.03 – 30 nM) in 1 ml RPMI 1640 containing 0.5% w/v bovine serum albumin (BSA). Non-specific binding was determined by coincubation with 100 µM PSMA I&T. After incubation, cells were washed with PBS and the cell-associated activity was measured in a shielded well-type gamma counter. The specific binding (total binding – nonspecific binding) was plotted against the bound/free ratio. Data were

analyzed by linear regression to determine PSMA antigen density per cell and to determine the K_d of ^{111}In-PSMA I&T.

Autoradiography

Binding of ^{111}In-PSMA I&T to 10-µm frozen sections of patient-derived xenografts (PDXs) and of human and mouse kidneys was evaluated using autoradiography. Tissue sections were preincubated for 5 min in ice-cold binding buffer (5 mM $MgCl_2$, 167 mM tris(hydroxymethyl)aminomethane hydrochloride, pH 7.6), followed by incubation for 1 h with ^{111}In-PSMA I&T (10^{-9} M) in binding buffer containing 1% w/v BSA. After incubation, the sections were washed successively with ice-cold binding buffer with 0.25 % w/v BSA for 5 min, binding buffer without BSA for 5 min, and ice-cold Ultrapure water for 5 s. Dried sections were placed in apposition to phosphor screens (PerkinElmer, Super Resolution) for 1 day. Radioactivity was assessed using a phosphor imager system (Cyclone, Packard, model A431201) and quantified using Optiquant software (PerkinElmer, Waltham, MA).

Animal studies

Animal experiments were performed in male BALB/c nude mice (Janvier, le Genest-Saint-Isle, France) and were conducted in accordance with the principles laid out by the revised Dutch Act on Animal Experimentation (1997) and approved by the institutional Animal Welfare Committee of the Radboud University Nijmegen. At 6-8 weeks of age, mice were inoculated subcutaneously with 3 x 10^6 LNCaP cells (in RPMI-1640 medium:matrigel 2:1, BD Biosciences, Pharmingen) and/or 2.5 x 10^6 LS174T in RPMI-1640 medium. Because LS174T-PSMA xenografts showed better tumor take and more reproducible growth, the LS174T-PSMA model was selected for pharmacokinetic and therapeutic experiments. The tracer was injected when tumors reached a size of approximately 0.1 cm^3. For SPECT/CT imaging of intraperitoneal tumors, mice were inoculated with 1 x 10^6 LS174T-PSMA cells in RPMI-1640 medium intraperitoneally and imaged 2-3 weeks after inoculation.

Dose escalation study

Four groups of five mice with subcutaneous PSMA-expressing xenografts (right flank: LNCaP, left flank: LS174T-PSMA) received an intravenous injection of 0.2 MBq ^{111}In-PSMA I&T (specific activity 2 MBq/nmol) in vehicle (PBS/ 0.5% BSA) in the tail vein. The effect of the dose of PSMA I&T on the biodistribution of ^{111}In-PSMA I&T was studied by administering different doses (0.1 – 0.3 – 1 – 10 nmol/mouse) to groups of five mice. Two hours post injection, mice were euthanized using CO_2/O_2-asphyxiation and the biodistribution of ^{111}In-PSMA I&T was determined ex vivo. Tumors, blood, and relevant organs and tissues were dissected, weighed, and radioactivity in each sample was quantified using a γ-counter. The results were expressed as percentage of injected dose per gram of tissue (%ID/g).

Reduction of renal tracer uptake with 2-PMPA

Five groups of five mice with subcutaneous LS174T-PSMA and LNCaP xenografts received an intravenous injection of 0.2 MBq ^{111}In-PSMA I&T (0.3 nmol) in vehicle in the tail vein. Mice were injected with either ^{111}In-PSMA I&T alone or in combination with 2-PMPA (10, 20, 50 nmol) to reduce specific binding in kidneys. One additional group was injected with 4 mg gelofusine 6 min before injection of ^{111}In-PSMA I&T to investigate tubular reabsorption mediated renal uptake. Two hours after injection, mice were euthanized and the biodistribution was determined ex vivo.

To determine the best time point of 2-PMPA injection, five groups of five mice with subcutaneous LS174T-PSMA xenografts received an intravenous injection of 0.2 MBq ^{111}In-PSMA I&T (0.3 nmol) with a preinjection (15 or 60 min), a coinjection, or a postinjection (15 or 60 min) of 50 nmol of 2-PMPA. Two hours after injection, mice were euthanized and the biodistribution was determined ex vivo.

Pharmacokinetics

To determine the pharmacokinetics of ^{111}In-PSMA I&T, eight groups of four mice with subcutaneous LS174T-PSMA xenografts received an intravenous injection of 0.2 MBq ^{111}In-PSMA I&T (0.3 nmol) in vehicle followed by ex vivo biodistribution at 1, 4, 24, and 48 h after injection. Mice were injected with or without 2-PMPA (50 nmol) coinjection to study the effect of 2-PMPA on tumor and kidney retention of ^{111}In-PSMA I&T.

SPECT/CT imaging

Mice with subcutaneous (n = 4) or intraperitoneal (n = 12) LS174T-PSMA tumors were injected intravenously with 20 MBq ^{111}In-PSMA I&T (0.3 nmol, specific activity 67 MBq/nmol) in vehicle, with or without coinjection of 2-PMPA (50 nmol). One hour after injection, mice were euthanized by CO_2/O_2 asphyxation and images were acquired with the U-SPECT-II/CT (MILabs, Utrecht, The Netherlands) [30]. Mice were scanned for 50 min using the 1.0 mm diameter pinhole mouse high sensitivity collimator tube, followed by a CT scan (spatial resolution 160 µm, 65 kV, 615 µA) for anatomical reference. Scans

were reconstructed with MILabs reconstruction software, using an ordered-subset expectation maximization algorithm, energy window 154 – 188 kEv, 3 iterations, 16 subsets, voxel size of 0.2 mm, and Gaussian filter 0.4 mm. SPECT/CT scans were analyzed and maximum intensity projections (MIPs) were created using the Inveon Research Workplace software (IRW, version 4.1).

Dosimetry

Biodistribution data obtained in the pharmacokinetic study were used to estimate the absorbed radiation doses to the organs and tumor. A single-exponential expression was fitted to the activity data at 1, 4, 24 and 48 h, and the cumulative activity concentration in each organ was calculated by analytic integration of the fitted expression.

Absorbed doses to the organs were calculated according to the MIRD-scheme [31] with the following equation: $D(r_T) = \sum_{r_S} \tilde{A}(r_S) \times S(r_T \leftarrow r_S)$, with $D(r_T)$ the absorbed dose to a target organ r_T, $\tilde{A}(r_S)$ the time-integrated activity in a source organ r_S and $S(r_T \leftarrow r_S)$ the absorbed dose rate per unit activity of ^{177}Lu. The S-values were obtained for a standardized 25 g mouse from the RADAR realistic animal models [32]. The biodistribution data were measured in activity concentration and hence the time-integrated activity concentration was obtained and this was multiplied with the source organ mass, as used in the phantom for the S-value calculation. The dosimetry calculations assume comparable biodistribution of ^{111}In-PSMA I&T and ^{177}Lu-PSMA I&T. Absorbed doses to renal cortex were estimated assuming localization of ^{177}Lu-PSMA I&T in the cortex [33].

Radionuclide therapy

To assess potential renal toxicity of ^{177}Lu-PSMA I&T, three groups of four mice with subcutaneous LS174T-PSMA xenografts were injected intravenously with 100 MBq ^{177}Lu-PSMA I&T (0.35 nmol) in vehicle with or without 2-PMPA (50 nmol) coinjection, or with vehicle (PBS/ 0.5% BSA). Body weight was monitored twice weekly. Renal function was assessed three months after treatment by quantification of renal uptake of ^{99m}Tc-dimercaptosuccinic acid (^{99m}Tc-DMSA) using SPECT [34] and by measuring plasma creatinine levels. DMSA (Renocis, IBA Molecular, The Netherlands) was radiolabeled with $^{99m}TcO_4^-$, which was eluated from a ^{99}Mo/^{99m}Tc-generator (GE Healthcare, The Netherlands). Mice were injected with 29 ± 5 MBq ^{99m}Tc-DMSA and images were acquired with the U-SPECT-II/CT, 2 h post injection, 20 min acquisition, scan range of 2.6 x 2.6 x 5.2 cm, using the 1.0 mm diameter pinhole mouse high sensitivity collimator tube. Scans were reconstructed with MILabs reconstruction software, using an ordered-subset expectation maximization algorithm, energy window 126-154 kEv, 3 iterations, 16 subsets, voxel size of 0.2 mm, and Gaussian filter 0.4 mm. Standards containing ^{99m}Tc-DMSA (0.036-3.36 MBq) were scanned using the same scanning protocol and a standard curve was derived for quantification. Scans were quantified by drawing a volume of interest (VOI) around the kidneys using the IRW software. Four days prior to scanning, plasma samples were collected and creatinine levels were analyzed by Aeroset (Abbott Diagnostics). Endpoint criteria were defined as body weight loss of > 20% of the initial body weight or body weight loss of > 15% within two days. One mouse reached a humane endpoint criterion 111 days after the start of therapy. The other mice were euthanized 118 days after the start of therapy for histopathological analysis of the kidneys. Two-µm sections of paraffin-embedded kidneys were stained with periodic acid Schiff following routine diagnostic procedures and analyzed for morphological alterations by an experienced pathologist (MC).

To determine the therapeutic efficacy of ^{177}Lu-PSMA I&T, three groups of ten mice with subcutaneous LS174T-PSMA xenografts were injected intraveneously with 100 MBq ^{177}Lu-PSMA I&T (0.35 nmol) in vehicle with or without 2-PMPA (50 nmol) coinjection, or with vehicle (PBS/ 0.5% BSA). Tumor growth was monitored by caliper measurements in three dimensions twice weekly. Body weight was monitored twice weekly. Endpoint criteria were defined as (1) body weight loss of > 20% of the initial body weight or body weight loss of > 15% within two days, (2) tumor volume of 2000 mm^3, (3) ulceration of the tumor.

Statistical analysis

Statistical analyses were performed using PASW Statistics version 18.0 (Chicago, IL) and GraphPad Prism version 5.03 (San Diego, CA). Differences in uptake of ^{111}In-PSMA I&T were tested for significance using the nonparametric Kruskal-Wallis and Mann-Whitney U test. Survival was described with the median survival, and survival curves were compared with the log-rank test. A p-value below 0.05 was considered significant.

Results

^{111}In-PSMA I&T shows high specificity to PSMA-expressing PCa cells, PCa xenografts, and kidneys in vitro

Binding of ^{111}In-PSMA I&T was assessed in vitro

on LNCaP and LS174T-PSMA cells in saturation binding experiments. The equilibrium binding constant (K_d) of ^{111}In-PSMA I&T was 3.9 ± 1.2 nM for LNCaP and 5.6 ± 1.2 nM for LS174T-PSMA. The number of ^{111}In-PSMA I&T binding sites was 137,000 ± 13,000 sites/cell for LNCaP and 43,000 ± 6,000 sites/cell for LS174T-PSMA.

Binding of ^{111}In-PSMA I&T was also evaluated on frozen xenograft tumors and kidney sections using autoradiography as shown in Fig. 2. ^{111}In-PSMA I&T showed high binding to all PSMA-expressing xenograft sections (LNCaP, PC310, PC346c, PC295 and PC82) and PSMA-expressing kidneys (mouse and human). Binding to LNCaP tumors was 6 times higher than binding to human kidneys and binding to mouse kidney was 2 times higher than binding to human kidneys. Binding to tumors showing no or very low expression of PSMA (PC3, VCaP, PC133, PC339, PC324) was very low, showing the target-specificity of the tracer.

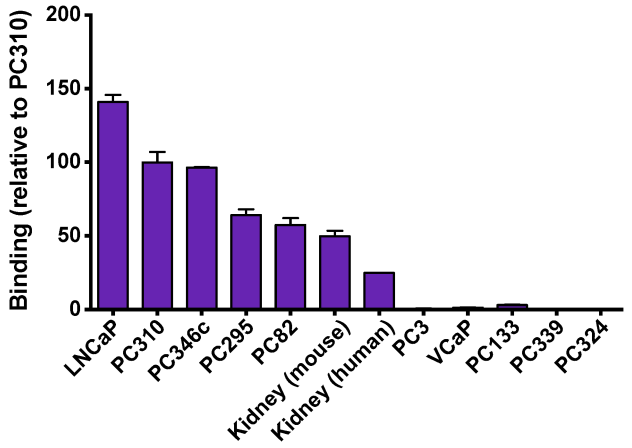

Figure 2. Specificity of ^{111}In-PSMA I&T for detecting PSMA-expressing tumors and tissues. High binding was observed on PSMA-expressing tumor sections (LNCaP, PC310, PC346c, PC295 and PC82) and PSMA-expressing kidneys (mouse and human), whereas no binding was observed to tumors showing no or very low expression of PSMA (PC3, VCaP, PC133, PC339, PC324).

^{111}In-PSMA I&T specifically accumulates in PSMA-expressing human xenografts in mice

The optimal tumor targeting doses of ^{111}In-PSMA I&T were 0.1 – 0.3 nmol for LS174T-PSMA tumors and 0.1 – 1.0 nmol for LNCaP tumors (Fig. 3A). Tumor uptake with 0.3 nmol ^{111}In-PSMA I&T was 17.0 ± 2.4 %ID/g and 11.7 ± 5.5 %ID/g for LS174T-PSMA and LNCaP, respectively (p = 0.095). Tumor uptake was significantly reduced from 0.3 nmol to 1 nmol tracer (p = 0.008) and from1 nmol to 10 nmol tracer (p = 0.008) for LS174T-PSMA and LNCaP, respectively. The tracer also specifically accumulated in kidneys, spleen, lungs, salivary glands, and adrenals. The highest uptake was measured in kidneys (122 ± 27.0 %ID/g for 0.3 nmol ^{111}In-PSMA I&T).

Coinjection of 2-PMPA significantly reduces renal uptake of ^{111}In-PSMA I&T

To reduce renal retention, different kidney protecting strategies were evaluated (Fig. 3B). Coinjection of 4 mg gelofusine did not significantly reduce renal uptake of ^{111}In-PSMA I&T (p = 0.42), whereas coinjection of 10 nmol 2-PMPA significantly reduced uptake in kidneys (p = 0.008), spleen (p = 0.016), lung (p = 0.032), adrenals (p = 0.032), and LS174T-PSMA tumors (p = 0.008), but not in LNCaP tumors (p = 0.310). The highest tumor-to-kidney ratios for LS174T-PSMA were obtained with 50 nmol 2-PMPA. Coinjection of 50 nmol 2-PMPA resulted in a 7-fold reduction in renal uptake (from 135.9 ± 31.2 %ID/g to 19.5 ± 1.8 %ID/g), whereas tumor uptake was only reduced 2-fold: from 14.9 ± 2.8 %ID/g to 6.8 ± 1.0 %ID/g (LS174T-PSMA) and from 11.0 ± 6.0 %ID/g to 5.4 ± 2.3 %ID/g (LNCaP). Timing of 2-PMPA injection significantly influenced the tumor/kidney tracer uptake ratios (p<0.001). Most effective renal tracer uptake reduction was obtained by coinjection of ^{111}In-PSMA I&T with 2-PMPA or preinjection of 2-PMPA 15 min before ^{111}In-PSMA I&T. Kidney/tumor tracer uptake ratio was significantly higher after coinjection as compared to 15 min preinjection (p = 0.008) of 2-PMPA (Fig. 3C).

Coinjection of 2-PMPA improves the tumor-to-kidney absorbed dose ratio

The optimal ^{111}In-PSMA I&T tracer dose (0.3 nmol) was selected to determine the tracer pharmacokinetics. Biodistribution studies were performed with and without 2-PMPA (coinjection of 50 nmol) for renal protection. For ^{111}In-PSMA I&T alone, uptake in tumor was the highest at 1 and 4 h after injection, and significantly decreased between 4 and 24 h after injection (p = 0.029) (Fig. 4A). For ^{111}In-PSMA I&T with 2-PMPA coinjection, tumor uptake was the highest at 1 h after injection and significantly decreased from 1 to 4 h after injection already (p = 0.029) (Fig. 4B). Uptake in PSMA-expressing healthy organs significantly decreased for both groups between 4 and 24 h after injection (p = 0.029).

Single-exponential curves were fitted to the biodistribution data and estimated absorbed doses to tumor and organs were calculated (Fig. 4C). Estimated absorbed doses from 100 MBq ^{177}Lu-PSMA I&T in tumor, kidneys, spleen, and adrenals were 36, 30, 1, and 2 Gy, respectively, for ^{177}Lu-PSMA I&T alone and 15, 5, 0.2, and 0.3 Gy, respectively, for ^{177}Lu-PSMA I&T with 2-PMPA. Tumor-to-kidney

dose ratio was substantially improved from 1.2 to 3.0 when ^{177}Lu-PSMA I&T was coinjected with 2-PMPA. Consequently, at an equivalent absorbed dose to the tumor (36 Gy), coinjection of 2-PMPA decreases absorbed dose to the kidneys from 30 Gy to 12 Gy. These absorbed doses to kidneys were calculated assuming uniform distribution of radioactivity. However, SPECT scans obtained 1 h after injection of ^{177}Lu-PSMA I&T clearly showed preferential localization of radioactivity in the renal cortex (Fig. S1). Therefore, dosimetric calculations were adjusted to estimate absorbed doses to renal cortex, taking into account this preferential localization of ^{177}Lu-PSMA I&T in the cortex. Absorbed doses to renal cortex were 44 and 7.3 Gy for ^{177}Lu-PSMA I&T alone and ^{177}Lu-PSMA I&T with 2-PMPA, respectively. Absorbed doses to other organs from 100 MBq of ^{177}Lu-PSMA I&T were below 1 Gy.

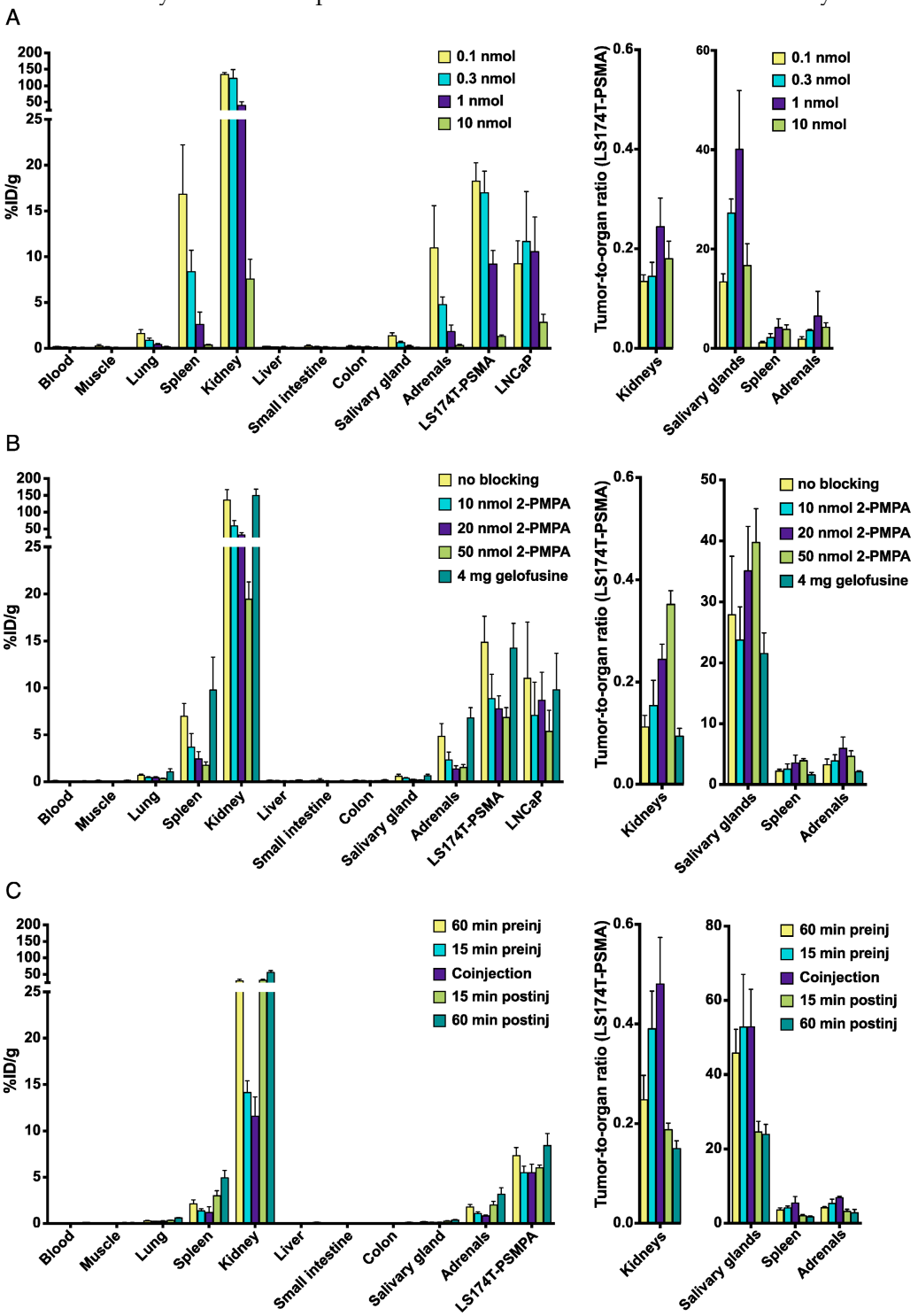

Figure 3. Biodistribution of ^{111}In-PSMA I&T in mice bearing LS174T-PSMA and LNCaP xenografts. Dose optimization (A), effect of 2-PMPA coinjection (10-50 nmol) or preinjection of gelofusine (B), and time schedule optimization of 2-PMPA injection (C) are depicted.

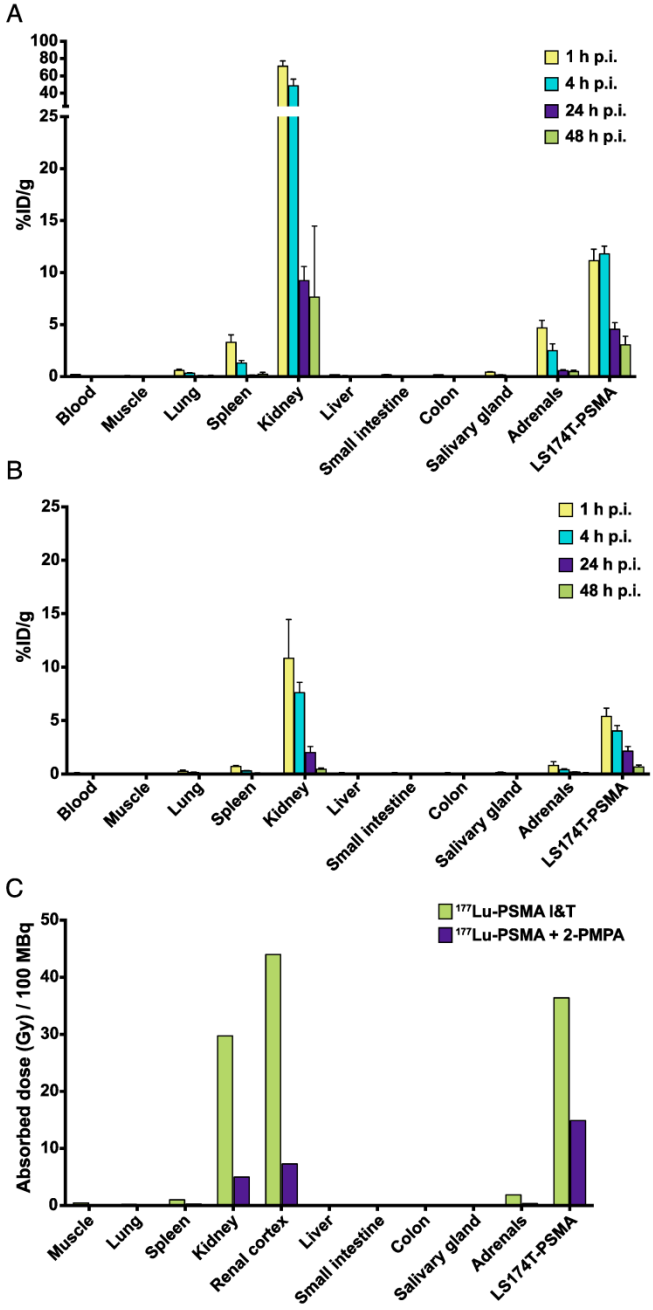

Figure 4. Pharmacokinetics and dosimetry of ^{111}In-PSMA I&T in mice bearing LS174T-PSMA xenografts. Biodistribution of ^{111}In-PSMA I&T (0.3 nmol) alone (A) or with coinjection of 50 nmol 2-PMPA (B) at different time points after injection. Absorbed doses (in Gy/100 MBq ^{177}Lu-PSMA I&T) were extrapolated from biodistribution data with and without 2-PMPA coinjection (C).

Coinjection of 2-PMPA improves visualization of metastatic tumor lesions located near kidneys and spleen

SPECT/CT imaging with ^{111}In-PSMA I&T, with or without 2-PMPA, clearly visualized subcutaneously growing LS174T-PSMA tumors and intraperitoneally growing LS174T-PSM metastases, whereas no uptake was observed in PSMA-negative LS174T tumors (Fig. 5A). High renal and spleen tracer uptake was observed in mice that did not receive coinjection of 2-PMPA, which interfered with visualization of metastases growing in the vicinity of these organs (Fig. 5B).

Coinjection of 2-PMPA protects from nephrotoxicity during ^{177}Lu-PSMA I&T radionuclide therapy

Non-tumor bearing mice treated with vehicle or ^{177}Lu-PSMA I&T + 2-PMPA gained body weight over 110 days (Fig. 6A). In contrast, an increase in body weight was observed up to 50 days for mice treated with ^{177}Lu-PSMA I&T only, followed by a slow decline in body weight up to 110 days. Three months after therapy, renal function was monitored by measuring renal uptake of ^{99m}Tc-DMSA and plasma creatinine levels. Renal uptake of ^{99m}Tc-DMSA was significantly reduced in mice treated with ^{177}Lu-PSMA I&T (1.0 ± 0.3 %ID/g) as compared to mice treated with vehicle (10.5 ± 1.0 %ID/g, $p<0.001$) or ^{177}Lu-PSMA I&T + 2-PMPA (9.8 ± 1.6 %ID/g, $p<0.001$) (Fig. 6B and 6C). Plasma creatinine levels were increased in mice treated with ^{177}Lu-PSMA I&T (8.2 ± 1.7 %ID/g) as compared to mice treated with vehicle (4.2 ± 1.6 %ID/g, $p = 0.029$) or ^{177}Lu-PSMA I&T + 2-PMPA (4.7 ± 2.1 %ID/g, $p = 0.114$) (Fig. 6D). Kidneys of mice treated with ^{177}Lu-PSMA I&T + 2-PMPA or vehicle showed normal morphology, whereas kidneys of mice treated with ^{177}Lu-PSMA I&T showed extensive cortical damage (Fig. 6E). Glomerular damage was denoted by segmental glomerular basement membrane thickening and wrinkling, and mesangial matrix increase, with pyknotic endothelial cells and podocytes. In addition, there was focal, global glomerular sclerosis. The tubular interstitial compartment of the cortex showed extreme acute tubular necrosis with atypia of the epithelial cells.

Therapeutic efficacy of ^{177}Lu-PSMA I&T is influenced by 2-PMPA

LS174T-PSMA tumor growth was significantly inhibited by 100 MBq of ^{177}Lu-PSMA I&T. A more effective growth inhibition was observed with ^{177}Lu-PSMA I&T alone as compared to ^{177}Lu-PSMA I&T + 2-PMPA. Mean doubling time for tumors of mice treated with vehicle, ^{177}Lu-PSMA, and ^{177}Lu-PSMPA + 2-PMPA were 6.1 ± 1.1 days, 13.9 ± 1.7 days, and 7.3 ± 1.7 days, respectively (Fig. 7A). Median survival for these groups was 13 days, 29 days, and 19 days, respectively ($p<0.0001$, Fig. 7B). Median survival significantly decreased in the group that received 2-PMPA in comparison with ^{177}Lu-PSMA I&T alone ($p = 0.0007$).

Discussion

A theranostic approach for detection, staging, treatment, and follow-up of PCa would be highly valuable to achieve personalized PCa treatment. PSMA is a very interesting target for such a theranostic approach, due to its consistent overexpression on PCa at all stages of disease. In recent years the number of PSMA-targeted agents for diagnostics and therapeutic applications has increased tremendously [35]. Currently, two theranostic PSMA-ligands are being evaluated in the clinic, namely PSMA I&T [25-27] and PSMA-617 [23, 36-38]. These 2 compounds contain an identical urea-binding motif, but have a different linker and chelator (Fig. 1). PSMA I&T contains a DOTAGA chelator, whereas PSMA-617 contains a DOTA chelator. The DOTAGA chelator and the presence of a 3-iodo-D-tyrosine in the linker of PSMA I&T have shown a favorable effect on the binding properties of urea-based small-molecule PSMA inhibitors [24, 25]. PSMA I&T and PSMA-617 have been shown to efficiently detect PCa lesions with high contrast, but also display very high uptake in kidneys and salivary glands, which raises concerns regarding potential toxicity during radionuclide therapy. Preliminary results of ^{177}Lu-PSMA-617 therapy in patients showed no acute renal insufficiencies in 2 months follow-up time, but longer follow-up is needed to get more insight into late-stage renal toxicity [36]. Similarly, no evidence of renal insufficiencies was reported for patients treated with ^{177}Lu-PSMA I&T over a follow-up period of at least 6 months [39]. In this study, 56 patients with progressive mCRPC received 1-5 cycles of ^{177}Lu-PSMA I&T, with a median administered activity per cycle of 5.76 GBq (3.6-8.7 GBq), and no significant change in serum creatinine level was observed after therapy.

Our study aimed to investigate the impact of healthy tissue uptake on the theranostic potential of PSMA I&T for SPECT imaging and radionuclide therapy of PCa. Our data showed that ^{111}In-PSMA I&T accumulated in PSMA-positive tumors, but not in PSMA negative tumors. In addition, PSMA-mediated uptake was observed in several normal murine tissues, including kidneys, spleen, salivary glands, adrenals, and lungs, of which kidneys showed the highest uptake. Our biodistribution data of ^{111}In-PSMA I&T were consistent with previously published data for ^{177}Lu-PSMA I&T [25]. Moreover, we show that uptake of ^{111}In-PSMA I&T in PSMA-expressing tissues can be blocked by coinjection of 2-PMPA in a dose-dependent manner, with the highest effect being obtained in the kidneys. Coadministration of 2-PMPA significantly reduced tumor uptake as well, but to a lower extent than kidney uptake, resulting in increased tumor-to-kidney ratios at all doses tested. Hillier et al. have shown that coinjection of 50 mg/kg 2-PMPA, a phosphonate-based PSMA inhibitor, nearly completely blocked tumor and kidney uptake of the PSMA inhibitor [^{123}I]MIP1095 [40]. More recently, Kratochwil et al. have shown the potential of 2-PMPA to selectively block kidney uptake without reducing tumor uptake by injecting 2-PMPA (0.2 – 50 mg/kg) 1 or 16 hours after injection of the PSMA inhibitors ^{99m}Tc-MIP1404 and ^{125}I-MIP1095, respectively [41]. They reported rapid and efficient displacement of renal tracer uptake with minimal effects on tumor uptake and suggested that a higher internalization rate by tumor cells in comparison with renal cells could explain these differential effects on tumor and kidneys.

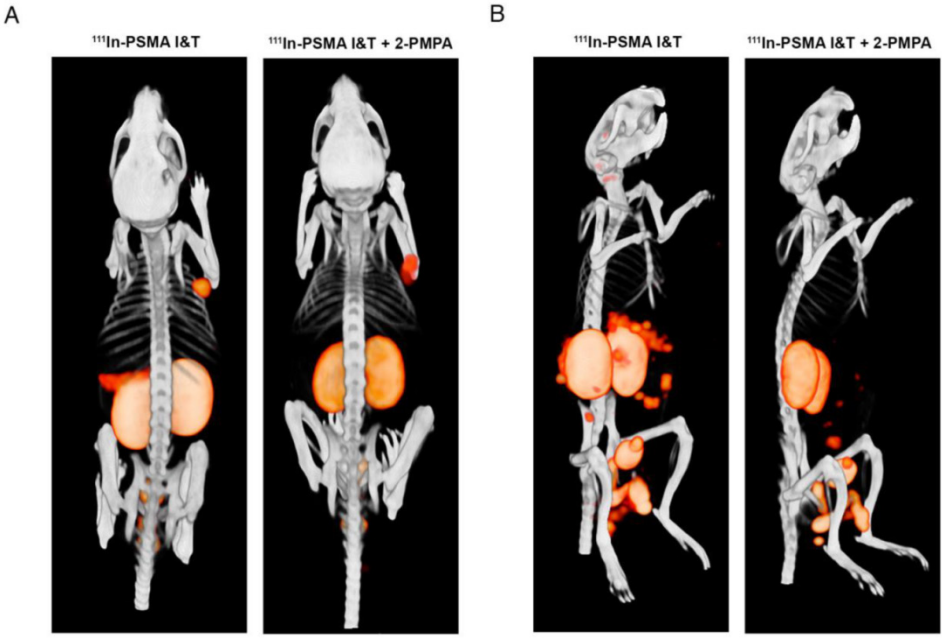

Figure 5. SPECT/CT imaging of ^{111}In-PSMA I&T in PSMA-expressing xenografts. (A) Representative SPECT/CT images of subcutaneous LS174T-PSMA xenografts (right shoulder) and LS174T (left shoulder) 1 h after injection of ^{111}In-PSMA I&T (0.3 nmol, 20 MBq) without (left) or with (right) coinjection of 50 nmol 2-PMPA. (B) Representative SPECT/CT images of intraperitoneal metastatic lesions of LS174T-PSMA cells 1 h after injection of ^{111}In-PSMA I&T (0.3 nmol, 20 MBq) without (left) or with (right) coinjection of 50 nmol 2-PMPA. Metastatic lesions were located around intestines, spleen and pancreas. High signal intensity in kidneys and spleen interfered with visualization of metastases in this area when 2-PMPA was not administered.

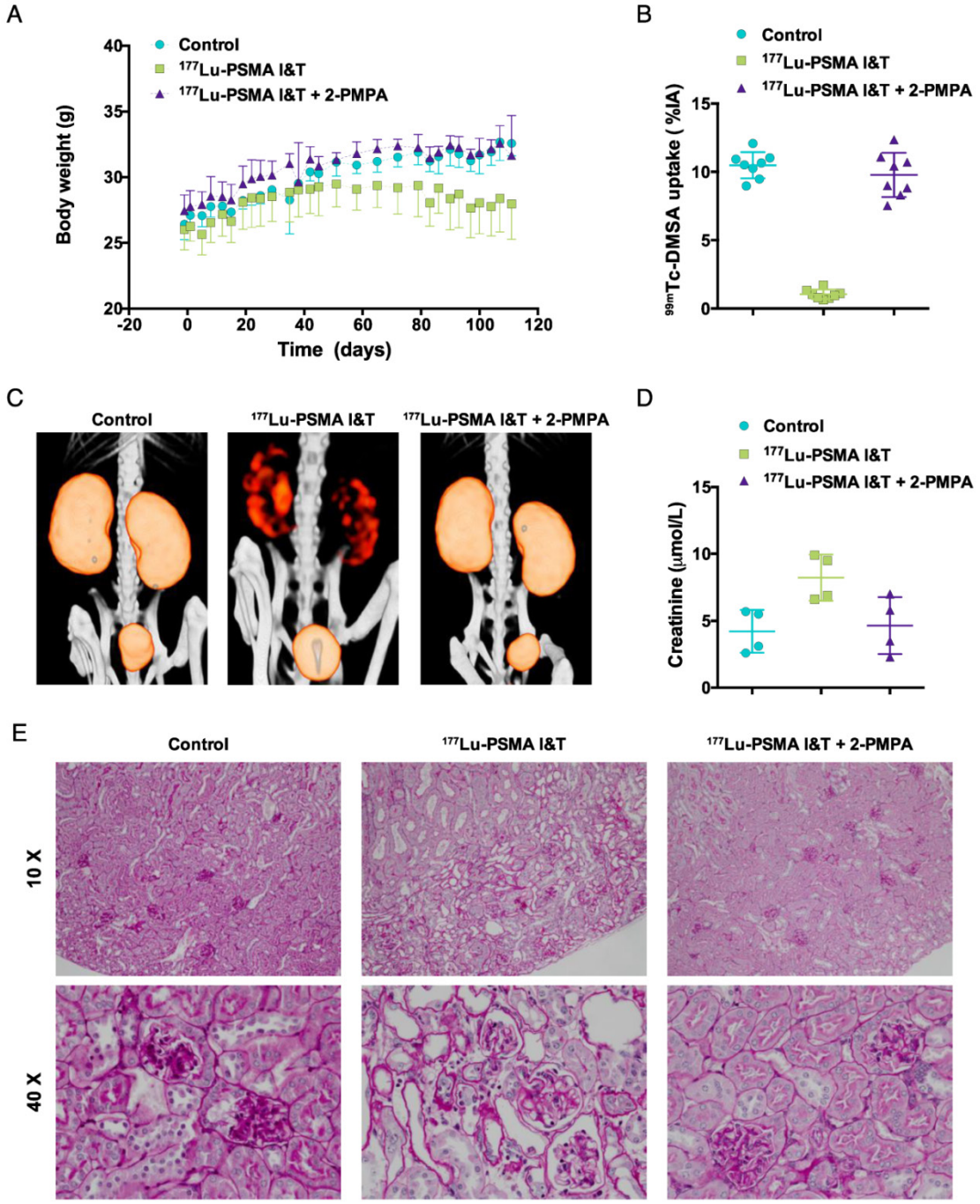

Figure 6. Toxicity of ^{177}Lu-PSMA I&T in non-tumor bearing mice. Mice (n = 4 per group) were treated with ^{177}Lu-PSMA I&T (100 MBq, 0.35 nmol) with or without 2-PMPA (50 nmol) on day 0. Control mice were injected with vehicle. Body weight follow-up (A), quantification of ^{99m}Tc-DMSA uptake (B), ^{99m}Tc-DMSA SPECT/CT scans (C), plasma creatinine levels (D), and periodic acid Schiff stained kidneys from treated mice (E) are displayed. Body weight loss, decreased renal uptake of ^{99m}Tc-DMSA, and increased plasma creatinine levels are observed for the group treated with ^{177}Lu-PSMA I&T without 2-PMPA. Kidneys of mice treated with ^{177}Lu-PSMA I&T + 2-PMPA or vehicle show normal morphology, whereas kidneys of mice treated with ^{177}Lu-PSMA I&T show extensive cortical damage. Tubular damage can be visualized by loss of epithelial cells and atypia of the remaining cells (10 X image). In addition, glomerular damage can be visualized by endothelial cell and podocyte pyknosis, focal glomerular basement membrane wrinkling and mesangial matrix increase (40 X image).

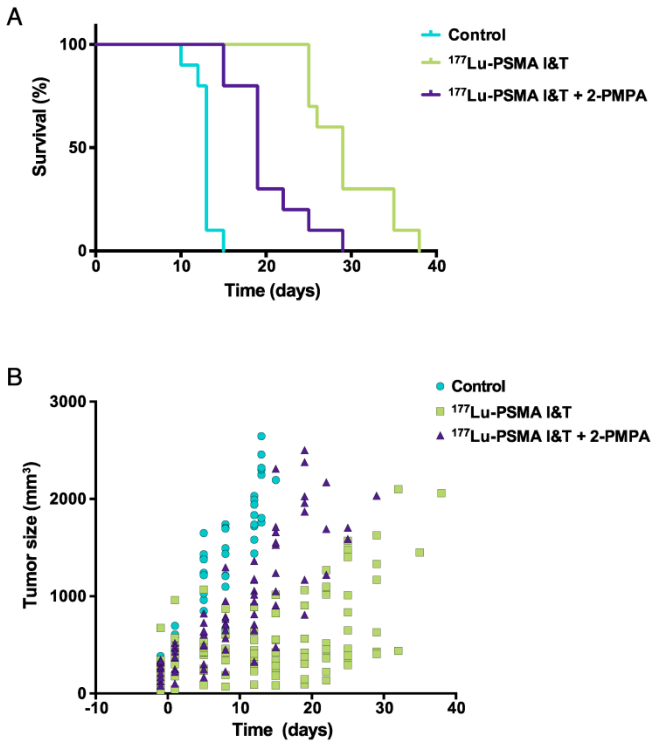

Figure 7. Therapeutic efficacy of ^{177}Lu-PSMA I&T in LS174T-PSMA tumors. Mice (n = 8 per group) were treated with ^{177}Lu-PSMA I&T (100 MBq, 0.35 nmol), with or without coinjection of 2-PMPA (50 nmol) on day 0. Control mice were injected with vehicle. Kaplan-Meier survival curves (A) and tumor size follow-up (B) are displayed.

In contrast with data obtained by Kratochwil et al. for ^{125}I-MIP1095 and ^{99m}Tc-MIP1404, injection of 2-PMPA (50 nmol per 25 g mouse ~ 0.45 mg/kg) 1 hour after injection of ^{111}In-PSMA I&T did not reduce renal uptake. In our study, only coinjection or 15 min preinjection resulted in effective inhibition of ^{111}In-PSMA I&T renal uptake. This resulted in a 7-fold reduction in renal uptake at 2 h after injection, whereas tumor uptake was reduced only by a factor of two. The differential effect on tumor and kidneys might be explained by differences in the kinetics of tumor and renal uptake of 2-PMPA and PSMA I&T. Because of its small size (Mw = 226 g/mol), high hydrophilicity, and low tissue penetration [42], 2-PMPA might be cleared rapidly from the circulation, resulting in higher accumulation in kidneys than in tumor. Additional studies are needed to determine the kinetics of 2-PMPA uptake in tumor and kidneys, providing more insight into this mechanism and facilitating optimization of 2-PMPA injection schedule in patients. Pre- or coinjection of blocking agents is preferred over postinjection, because the kidneys will be protected from radiation-induced damage from the start of therapy, which could be especially beneficial with short half-life radionuclides, e.g. ^{213}Bi.

In the case of application of PSMA inhibitors for PET imaging, high uptake observed in kidneys and salivary glands is not of major concern for detection of primary tumors or distant metastases. However, if metastases are situated in the vicinity of organs showing tracer uptake, this could interfere with the interpretation of the images. Our metastatic model indicates that coinjection of ^{111}In-PSMA I&T with 2-PMPA improved the visualization of intraperitoneal tumor lesions in the vicinity of kidneys, adrenals, and spleen.

For PSMA-targeted radionuclide therapy, high uptake observed in kidneys and salivary glands are major concerns. To investigate the potential protective effect of 2-PMPA on renal toxicity, a therapeutic study was performed with 100 MBq ^{177}Lu-PSMA I&T with and without coinjection of 2-PMPA. Several groups have reported radiation-induced nephropathy in mice between 15 and 30 weeks after therapy using ^{177}Lu-labeled therapeutic agents, translating into reduced ^{99m}Tc-DMSA clearance and increased serum creatinine levels [33, 43, 44]. Svensson et al. have reported a threshold dose value of 24 Gy to renal cortex for ^{177}Lu-DOTATATE in nude mice [33]. In our study, estimated absorbed doses to renal cortex were 44 Gy and 7.3 Gy, for ^{177}Lu-PSMA I&T and ^{177}Lu-PSMA I&T + 2-PMPA, respectively. Consistently, nephrotoxicity was observed in mice treated with 100 MBq ^{177}Lu-PSMA I&T at 3 months after start of therapy, as shown by the decreased ^{99m}Tc-DMSA uptake and increased serum creatinine levels. On the contrary, nephrotoxicity was not observed when 2-PMPA was coadministered.

Therapeutic efficacy of ^{177}Lu-PSMA I&T was significantly reduced by coinjection of 2-PMPA, which can be explained by the 2-fold higher dose delivered to the tumor cells for ^{177}Lu-PSMA I&T alone in comparison with ^{177}Lu-PSMA I&T with 2-PMPA. To improve therapeutic efficacy, the dose delivered to the tumor for ^{177}Lu-PSMA I&T with 2-PMPA could be increased by administering a double dose of ^{177}Lu-PSMA I&T. This would result in an estimated absorbed dose of 30 Gy to the tumor and 14.6 Gy to the renal cortex, provided that receptor saturation has not been reached. Alternatively, 2 doses of ^{177}Lu-PSMA I&T could be administered at an interval allowing clearance of the tracer.

These preclinical results illustrate the potential of PSMA I&T for theranostic approaches in PCa. However, the extrapolation of these data to the clinical situation should be performed carefully. Pitfalls might include differences in expression of PSMA in human and its murine homolog Folh1 in mice, differences in affinities for PSMA expressed on human (xenograft) tumors and Folh1 expressed on murine tissues, and differences in pharmacokinetics

in mice and humans. Due to differences in expression pattern of Folh1 in mouse organs and PSMA in human organs, further studies should be performed in patients to determine the effect of 2-PMPA blocking on normal organs showing high PSMA expression, such as the salivary glands and kidneys. Even though no evidence of nephrotoxicity was observed in the first studies with high doses of ^{177}Lu-PSMA I&T in patients, further investigations to reduce the dose to kidneys and salivary glands in patients might enhance the maximum tolerable dose and improve the therapeutic window.

Moreover, safety and pharmacokinetics of 2-PMPA should be tested in patients. In preclinical models, PSMA inhibitors have shown utility for treatment of neurological diseases in which excessive excitatory glutamate transmission is pathogenic [45]. Indeed, PSMA inhibition could limit detrimental excess glutamate release in the nervous system, by blocking conversion of N-acetylaspartylglutamate into glutamate. Importantly, PSMA inhibition had no effect on basal glutamate transmission in healthy animals [46]. Even though 2-PMPA has shown high affinity and selectivity towards PSMA, it was not evaluated in patients because of its poor oral bioavailability and limited brain penetration. A more lipophilic PSMA inhibitor, 2-(-3-mercaptopropyl) pentanedioic acid, which is almost as potent as 2-PMPA, was found to be safe and well tolerated in healthy subjects [47]. For our application, however, the use of a hydrophilic PSMA inhibitor with poor brain penetration would be preferred, because it would less likely induce adverse events. In conclusion, future research is warranted to address the identified pitfalls and translate this concept in PCa patients.

In conclusion, PSMA I&T is a highly promising theranostic agent for radionuclide imaging and therapy of PCa. Coinjection of 2-PMPA efficiently reduced renal uptake, thereby improving visualization of intraperitoneal tumor lesions in the vicinity of kidneys, adrenals, and spleen and protecting from nephrotoxicity after radionuclide therapy. Because 2-PMPA also reduced tumor uptake, it might hamper therapeutic efficacy, which could be resolved by increasing amounts of injected activity.

Supplementary Material

Supplementary figure.
http://www.thno.org/v06p0849s1.pdf

Acknowledgment

The authors thank Danny Gerrits, Cathelijne Frielink, Bianca Lemmers – van de Weem, Iris Lamers-Elemans, Kitty Lemmens-Hermans, and Sharon Wennekers for their assistance during animal experiments. Funding: Drs. Chatalic is employed on a project funded by the Erasmus MC grant "Novel Radio-Antagonists for PET/MRI Imaging and Therapy of Prostate Cancer".

Author contributions

The project was supervised by MdJ and OCB. The study was designed by KLSC, SH, WMvW, MdJ and OCB. Data acquisition was performed by KLSC, SH, JDMM, and GMF. Data analysis was performed by KLSC, SH, and MK. KLSC and SH wrote the manuscript draft. MS and HJW contributed to the design of PSMA I&T and edited the manuscript. All authors reviewed and edited the intermediate and final versions of the manuscript.

Competing Interests

HJW owns shares with the radiopharmaceutical company Scintomics.

References

1. Siegel R, DeSantis C, Virgo K, et al. Cancer treatment and survivorship statistics, 2012. CA Cancer J Clin. 2012; 62: 220-41.
2. Heidenreich A, Bastian PJ, Bellmunt J, et al. EAU guidelines on prostate cancer. Part II: Treatment of advanced, relapsing, and castration-resistant prostate cancer. Eur Urol. 2014; 65: 467-79.
3. Heidenreich A, Porres D. Prostate cancer: treatment sequencing for CRPC--what do we know? Nat Rev Urol. 2014; 11: 189-90.
4. Hoskin P, Sartor O, O'Sullivan JM, et al. Efficacy and safety of radium-223 dichloride in patients with castration-resistant prostate cancer and symptomatic bone metastases, with or without previous docetaxel use: a prespecified subgroup analysis from the randomised, double-blind, phase 3 ALSYMPCA trial. Lancet Oncol. 2014; 15: 1397-406.
5. Humm JL, Sartor O, Parker C, et al. Radium-223 in the treatment of osteoblastic metastases: a critical clinical review. Int J Radiat Oncol Biol Phys. 2015; 91: 898-906.
6. Bostwick DG, Pacelli A, Blute M, et al. Prostate specific membrane antigen expression in prostatic intraepithelial neoplasia and adenocarcinoma: a study of 184 cases. Cancer. 1998; 82: 2256-61.
7. Silver DA, Pellicer I, Fair WR, et al. Prostate-specific membrane antigen expression in normal and malignant human tissues. Clin Cancer Res. 1997; 3: 81-5.
8. Wright GL, Jr., Haley C, Beckett ML, et al. Expression of prostate-specific membrane antigen in normal, benign, and malignant prostate tissues. Urol Oncol. 1995; 1: 18-28.
9. Wright GL, Jr., Grob BM, Haley C, et al. Upregulation of prostate-specific membrane antigen after androgen-deprivation therapy. Urology. 1996; 48: 326-34.
10. Ellis RJ, Kaminsky DA, Zhou EH, et al. Ten-year outcomes: the clinical utility of single photon emission computed tomography/computed tomography capromab pendetide (Prostascint) in a cohort diagnosed with localized prostate cancer. Int J Radiat Oncol Biol Phys. 2011; 81: 29-34.
11. Milowsky MI, Nanus DM, Kostakoglu L, et al. Phase I trial of yttrium-90-labeled anti-prostate-specific membrane antigen monoclonal antibody J591 for androgen-independent prostate cancer. J Clin Oncol. 2004; 22: 2522-31.
12. Tagawa ST, Beltran H, Vallabhajosula S, et al. Anti-prostate-specific membrane antigen-based radioimmunotherapy for prostate cancer. Cancer. 2010; 116: 1075-83.
13. Barrett JA, Coleman RE, Goldsmith SJ, et al. First-in-man evaluation of 2 high-affinity PSMA-avid small molecules for imaging prostate cancer. J Nucl Med. 2013; 54: 380-7.
14. Afshar-Oromieh A, Avtzi E, Giesel FL, et al. The diagnostic value of PET/CT imaging with the (68)Ga-labelled PSMA ligand HBED-CC in the diagnosis of recurrent prostate cancer. Eur J Nucl Med Mol Imaging. 2015; 42: 197-209.
15. Beheshti M, Kunit T, Haim S, et al. BAY 1075553 PET-CT for Staging and Restaging Prostate Cancer Patients: Comparison with [F] Fluorocholine PET-CT (Phase I Study). Mol Imaging Biol. 2014.
16. Pandit-Taskar N, O'Donoghue JA, Durack JC, et al. A Phase I/II Study for Analytic Validation of 89Zr-J591 ImmunoPET as a Molecular Imaging Agent for Metastatic Prostate Cancer. Clin Cancer Res. 2015.

17. Rowe SP, Gage KL, Faraj SF, et al. 18F-DCFBC PET/CT for PSMA-Based Detection and Characterization of Primary Prostate Cancer. J Nucl Med. 2015; 56: 1003-10.
18. Budaus L, Leyh-Bannurah SR, Salomon G, et al. Initial Experience of Ga-PSMA PET/CT Imaging in High-risk Prostate Cancer Patients Prior to Radical Prostatectomy. Eur Urol. 2015.
19. Szabo Z, Mena E, Rowe SP, et al. Initial Evaluation of [(18)F]DCFPyL for Prostate-Specific Membrane Antigen (PSMA)-Targeted PET Imaging of Prostate Cancer. Mol Imaging Biol. 2015; 17: 565-74.
20. Vallabhajosula S, Nikolopoulou A, Jhanwar YS, et al. Radioimmunotherapy of Metastatic Prostate Cancer with 177Lu-DOTA-huJ591 Anti Prostate Specific Membrane Antigen Specific Monoclonal Antibody. Curr Radiopharm. 2015.
21. Tagawa ST, Milowsky MI, Morris M, et al. Phase II study of Lutetium-177-labeled anti-prostate-specific membrane antigen monoclonal antibody J591 for metastatic castration-resistant prostate cancer. Clin Cancer Res. 2013; 19: 5182-91.
22. Zechmann CM, Afshar-Oromieh A, Armor T, et al. Radiation dosimetry and first therapy results with a (124)I/ (131)I-labeled small molecule (MIP-1095) targeting PSMA for prostate cancer therapy. Eur J Nucl Med Mol Imaging. 2014; 41: 1280-92.
23. Benesova M, Schafer M, Bauder-Wust U, et al. Preclinical Evaluation of a Tailor-Made DOTA-Conjugated PSMA Inhibitor with Optimized Linker Moiety for Imaging and Endoradiotherapy of Prostate Cancer. J Nucl Med. 2015; 56: 914-20.
24. Weineisen M, Simecek J, Schottelius M, et al. Synthesis and preclinical evaluation of DOTAGA-conjugated PSMA ligands for functional imaging and endoradiotherapy of prostate cancer. EJNMMI Res. 2014; 4: 63.
25. Weineisen M, Schottelius M, Simecek J, et al. 68Ga- and 177Lu-Labeled PSMA I&T: Optimization of a PSMA-Targeted Theranostic Concept and First Proof-of-Concept Human Studies. J Nucl Med. 2015; 56: 1169-76.
26. Herrmann K, Bluemel C, Weineisen M, et al. Biodistribution and radiation dosimetry for a probe targeting prostate-specific membrane antigen for imaging and therapy. J Nucl Med. 2015; 56: 855-61.
27. Maurer T, Weirich G, Schottelius M, et al. Prostate-specific membrane antigen-radioguided surgery for metastatic lymph nodes in prostate cancer. Eur Urol. 2015; 68: 530-4.
28. Lutje S, Rijpkema M, Franssen GM, et al. Dual-Modality Image-Guided Surgery of Prostate Cancer with a Radiolabeled Fluorescent Anti-PSMA Monoclonal Antibody. J Nucl Med. 2014; 55: 995-1001.
29. Brom M, Joosten L, Oyen WJ, et al. Improved labelling of DTPA- and DOTA-conjugated peptides and antibodies with 111In in HEPES and MES buffer. EJNMMI Res. 2012; 2: 4.
30. van der Have F, Vastenhouw B, Ramakers RM, et al. U-SPECT-II: An Ultra-High-Resolution Device for Molecular Small-Animal Imaging. J Nucl Med. 2009; 50: 599-605.
31. Bolch WE, Eckerman KF, Sgouros G, et al. MIRD pamphlet No. 21: a generalized schema for radiopharmaceutical dosimetry--standardization of nomenclature. J Nucl Med. 2009; 50: 477-84.
32. Keenan MA, Stabin MG, Segars WP, et al. RADAR realistic animal model series for dose assessment. J Nucl Med. 2010; 51: 471-6.
33. Svensson J, Molne J, Forssell-Aronsson E, et al. Nephrotoxicity profiles and threshold dose values for [177Lu]-DOTATATE in nude mice. Nucl Med Biol. 2012; 39: 756-62.
34. Forrer F, Valkema R, Bernard B, et al. In vivo radionuclide uptake quantification using a multi-pinhole SPECT system to predict renal function in small animals. Eur J Nucl Med Mol Imaging. 2006; 33: 1214-7.
35. Kiess A, Banerjee S, Mease R, et al. Prostate-Specific Membrane Antigen as a target for cancer imaging and therapy. Q J Nucl Med Mol Imaging. 2015.
36. Ahmadzadehfar H, Rahbar K, Kurpig S, et al. Early side effects and first results of radioligand therapy with (177)Lu-DKFZ-617 PSMA of castrate-resistant metastatic prostate cancer: a two-centre study. EJNMMI Res. 2015; 5: 114.
37. Kabasakal L, AbuQbeitah M, Aygun A, et al. Pre-therapeutic dosimetry of normal organs and tissues of Lu-PSMA-617 prostate-specific membrane antigen (PSMA) inhibitor in patients with castration-resistant prostate cancer. Eur J Nucl Med Mol Imaging. 2015.
38. Afshar-Oromieh A, Hetzheim H, Kratochwil C, et al. The novel theranostic PSMA-ligand PSMA-617 in the diagnosis of prostate cancer by PET/CT: biodistribution in humans, radiation dosimetry and first evaluation of tumor lesions. J Nucl Med. 2015.
39. Baum RP, Kulkarni HR, Schuchardt C, et al. Lutetium-177 PSMA Radioligand Therapy of Metastatic Castration-Resistant Prostate Cancer: Safety and Efficacy. J Nucl Med. 2016.
40. Hillier SM, Maresca KP, Femia FJ, et al. Preclinical evaluation of novel glutamate-urea-lysine analogues that target prostate-specific membrane antigen as molecular imaging pharmaceuticals for prostate cancer. Cancer Res. 2009; 69: 6932-40.
41. Kratochwil C, Giesel FL, Leotta K, et al. PMPA for nephroprotection in PSMA-targeted radionuclide therapy of prostate cancer. J Nucl Med. 2015; 56: 293-8.
42. Rais R, Rojas C, Wozniak K, et al. Bioanalytical method for evaluating the pharmacokinetics of the GCP-II inhibitor 2-phosphonomethyl pentanedioic acid (2-PMPA). J Pharm Biomed Anal. 2014; 88: 162-9.
43. Haller S, Reber J, Brandt S, et al. Folate receptor-targeted radionuclide therapy: preclinical investigation of anti-tumor effects and potential radionephropathy. Nucl Med Biol. 2015; 42: 770-9.
44. Reber J, Haller S, Leamon CP, et al. 177Lu-EC0800 combined with the antifolate pemetrexed: preclinical pilot study of folate receptor targeted radionuclide tumor therapy. Mol Cancer Ther. 2013; 12: 2436-45.
45. Rahn KA, Slusher BS, Kaplin AI. Glutamate in CNS neurodegeneration and cognition and its regulation by GCPII inhibition. Curr Med Chem. 2012; 19: 1335-45.
46. Slusher BS, Vornov JJ, Thomas AG, et al. Selective inhibition of NAALADase, which converts NAAG to glutamate, reduces ischemic brain injury. Nat Med. 1999; 5: 1396-402.
47. van der Post JP, de Visser SJ, de Kam ML, et al. The central nervous system effects, pharmacokinetics and safety of the NAALADase-inhibitor GPI 5693. Br J Clin Pharmacol. 2005; 60: 128-36.